# Experimental and Computational Study on $CuWO_4/WO_3$ Heterostructure for Solar Water Splitting

**R. Salimi[1,2], A.A. Sabbagh Alvani[* 1,2], H. Sameie[1,2], D. Poelman[3]**

[1] *Color & Polymer Research Center, Amirkabir University of Technology (Tehran Polytechnic), P.O. Box 15875-4413, Tehran, Iran*

[2] *Department of Polymer Engineering and Color Technology, Amirkabir University of Technology (Tehran Polytechnic), Tehran, Iran*

[3] *Lumilab, Department of Solid State Sciences, Ghent University, Belgium*

* *E-mail:* sabbagh_alvani@aut.ac.ir

**Abstract:** Sol-gel synthesis and electrophoretic deposition method were used to prepare $CuWO_4/WO_3$ thin film as photoanode for photoelectrochemical water splitting and characterized via experimental analyses and the first-principles calculations based on the density functional theory (DFT).

**OCIS codes**: (160.0160); (160.6000); (350.6050)

## 1. Introduction

In the past decades, photo-electrochemical (PEC) water splitting is frequently proposed as promising technology for production of hydrogen to solve global energy crisis and environment problems [1]. The development of low cost and environmentally benign materials that can harvest significant fractions of solar irradiation, efficiently create and separate charge carriers, and allow for electrochemical water reduction or oxidation, is one of the main challenges of ongoing research [2]. $CuWO_4$ has recently attracted interests to be a promising candidate for PEC applications [3, 4]. Its band gap (about 2.2-2.4 eV) has been shown to be the optimal value for water splitting in tandem devices and theoretically solar to hydrogen (STH) efficiencies of up to 13% are feasible [4]. Unfortunately, a high bulk charge transfer resistance (due to the empty orbital of Cu ($3dx^2$-$y^2$)) negatively affect the overall water splitting efficiency [5]. Various strategies such as the fabrication of heterostructured systems have been widely used to improve the PEC performance of $CuWO_4$-based photoanodes [3-6].

## 2. Experimental and computational procedure

A sol-gel (PSG) approach was used to prepare the products using $Cu(NO_3)_2.3H_2O$, ethylene glycol, AMT and PVP. Thin film photoanodes were prepared via electrophoretic deposition on FTO glass [7, 8]. PEC measurements were performed in a three-electrode configuration (VersaSTAT 4 potentiostat) using the obtained thin film samples as working electrode (exposed area of 0.28 $cm^2$). A Pt wire and a Ag/AgCl (saturated KCl) electrode were used as counter and reference electrode, respectively.

All DFT calculations are carried out using the Cambridge Serial Total Energy Package code (CASTEP) based on the total energy plane wave pseudopotentials approach [9]. The slabs are built by cleaving the bulk $WO_3$ and $CuWO_4$ (3×3×3 supercell for $CuWO_4$ and 2×2×2 supercell for $WO_3$) along the (110) planes, with the minimum lattice mismatch (less than 3%). In this study, the heterostructure is modelled by stacking a monolayer $WO_3$ (110) surface on top of the $CuWO_4$ (110) monolayer with a vacuum space of 20 Å to avoid interactions between the neighboring slabs in the z-direction. The Perdew-Burke-Ernzerhof (PBE) parameterization functional of the generalized gradient approximation (GGA) with DFT-D of van der Waals dispersion corrections (to accurate describe the nonbonding van der Waals interaction along c-axis) is used to treat the exchange-correlation effect. The Brillouin-zone integrations are implemented using the Monkhorst-Pack approach, with k-point sampling grids of 3 × 3 × 3 for geometry calculation, and a cut-off energy of 340 eV. The structural relaxations are performed until the maximum atomic force, atomic energy, maximum displacement become smaller than 0.3 eV $Å^{-1}$, $10^{-5}$ eV/atom and 0.01 Å, respectively [10].

## 3. Results and discussion

The optimized and calculated lattice constants of a = 4.774 Å, b = 5.982 Å, c = 4.941 Å for $CuWO_4$ (Pī space group) and a = 7.451 Å, b = 7.574 Å, c = 7.711 Å for $WO_3$ (P21/n space group) agree considerably well with experimentally determined lattice constants. The slight differences between calculated results and experimental measurements indicate that the computational method adopted in the present work could produce reliable results. The interaction between the individual monolayers of the hetero-structure is an essential factor in determining the photocatalytic stability and activity. To evaluate the stability of the hetero-structure, the interface binding energy is calculated according to eq. (1):

$$E_b = E_{CuWO4/WO3} - E_{CuWO4} - E_{WO3} \quad (1)$$

where $E_{CuWO4/WO3(110)}$, $E_{CuWO4}$ and $E_{WO3}$ are the total energy of the hetero-structure and the individual monolayers in the hetero-structure, respectively. The interfacial binding energy is calculated as -0.58 eV for

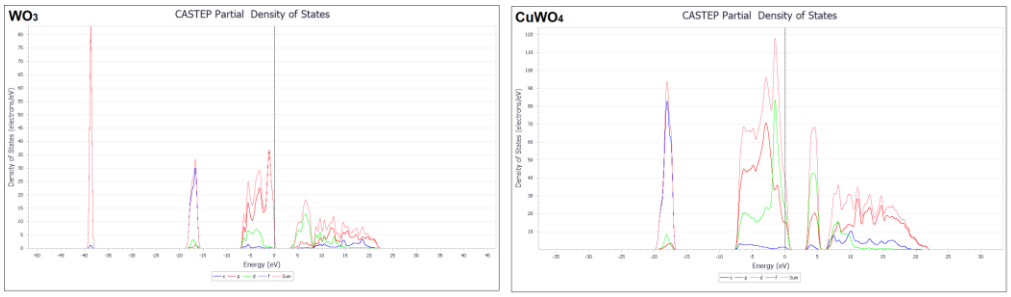


Fig. 1. Calculated PDOS of $CuWO_4$ (110) and $WO_3$ (110)

$CuWO_4/WO_3$ (110) hetero-structure which indicates a typical van der Waals interaction. The negative formation energy indicates that the heterojunction can form a stable interface (thermodynamically), thus, the formation of $WO_3$ on the $CuWO_4$ surface is exothermic and energetically favorable.

To investigate the effect of interfacial interaction and for qualitative insights into the interface electronic structure and identification of the orbital contributions, the projected density of state (PDOS) is analyzed (Fig .1). The PDOS analysis of pure $WO_3$ reveals that the VBM is predominantly contributed by O 2p states, while the CBM is composed of W 5d states with the computed band gap of 2.394 eV, relatively close to the experimental value (about 2.6 eV from UV-Vis data). However, the PDOS of pure $CuWO_4$ shows that the VBM largely occupied by O 2p with some contribution of Cu 3d and Cu 4s (Fig. 1). Thus, hybridization of the metal d-orbitals with the O (2p) valence band results in the lower calculated band gap (2.017 eV) compared to $WO_3$.

The work function is a crucial electronic parameter of any photocatalytic material, which determines the relative position of the Fermi level and also evaluates the charge transfer and the band alignment at the interface of hetero-structures. For a solid surface, it is calculated according to eq. (2):

$$\Phi = E_{vac} - E_F \quad (2)$$

where $E_{vac}$ and $E_F$ are the electrostatic potential of the vacuum and Fermi energy level, respectively. To comprehend the origin of charge transfer at the interface, the work function of the $CuWO_4$ (110) and $WO_3$ (110) surfaces are calculated and plotted (Fig. 2). The work functions of $WO_3$ (110) and $CuWO_4$ (110) and hetero-structure surfaces are estimated as 6.18, 5.65 and 5.78 eV, respectively, forming a type-II band alignment. Due to the different Fermi energies, electrons will flow from $CuWO_4$ to $WO_3$ (0.14 |e| calculated charge transfer according to Mulliken population charge analysis) when they are in contact, until the two Fermi energies reach the same level. Therefore, near the interface, the $WO_3$ and $CuWO_4$ will be negatively and positively charged, respectively. Afterwards, a built-in potential directed from $CuWO_4$ to the $WO_3$ can be formed after an equalized Fermi level is acquired. The interfacial electrostatic potential difference, which is the origin of the built-in potential is beneficial for the separation and migration of the charge carriers which can relatively reduce the recombination of photo-induced charge carriers in the hetero-structure. Hence, the photocatalytic stability and performance of $CuWO_4$ can be improved by incorporating with the $WO_3$ monolayer.

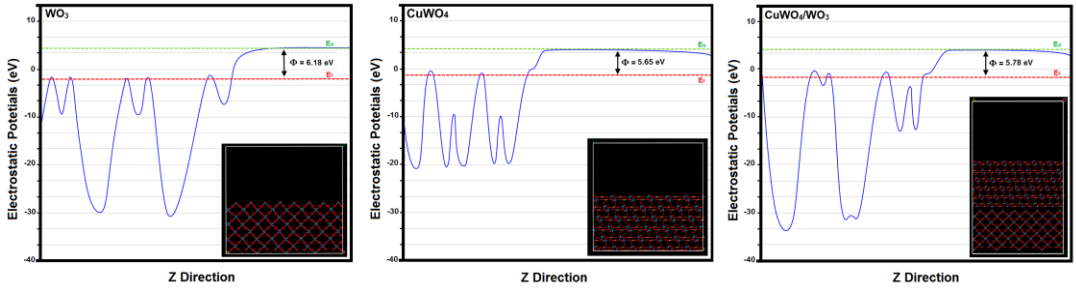


Fig. 2. Calculated electrostatic potential difference of $CuWO_4$ (110) slab, $WO_3$ (110) slab and $CuWO_4/WO_3$ (110) hetero-structure

The phase purity and crystallinity of the as-prepared materials were determined by X-ray diffraction (Fig. 3a), revealing the formation of both phases of $WO_3$ with a= 7.318 Å, b= 7.542 Å, c= 7.693 Å (JCPDS data card No. 43-1035) and $CuWO_4$ with $a$ = 4.692 Å, $b$ = 5.831 Å, $c$ = 4.879 Å estimated lattice parameters (JCPDS data card No. 72-0616) [8]. Fig. 3b depicts the UV-Vis spectra of the as-synthesized $CuWO_4/WO_3$ heterostructure, thereby the band-gaps of the $CuWO_4/WO_3$ heterostructure was estimated to be 2.28-2.33 eV. Effective hybridization of the metal $Cu^{2+}$ d-orbitals with the O (2p) valence band results in the lower band gap compared to pure $WO_3$. The photoluminescence (PL) emission was measured using a 340 nm laser for excitation (Fig. 3c). The radiative emission intensity of the heterostructures is evidently reduced compared to both pure $WO_3$ and $CuWO_4$, which assigned to an effective suppression of electron-hole recombination pathways due to the staggered band alignment with the charge transfer between $CuWO_4$ and $WO_3$, results in an interfacial built-in potential, which can favour the separation of charge carriers. Typical linear sweep voltammetry (LSV) scans obtained in potassium phosphate buffer solution (pH7) for front-side illuminated samples are presented in Fig. 3d,e,f. Independent on the exact composition of the electrode, for all samples a positive response to light-stimuli

was observed as evidenced by the generated anodic photocurrents. For pristine $WO_3$ and $CuWO_4$ films, a photocurrent density of approximately 0.048 and 0.075 mA/cm$^2$ at 0.62 V vs Ag/AgCl (thermodynamic redox potential for water oxidation) were measured. As expected for the composite electrode, $CuWO_4/WO_3$, a 2-3 times (0.152 mA/cm$^2$) higher photocurrent density was obtained.

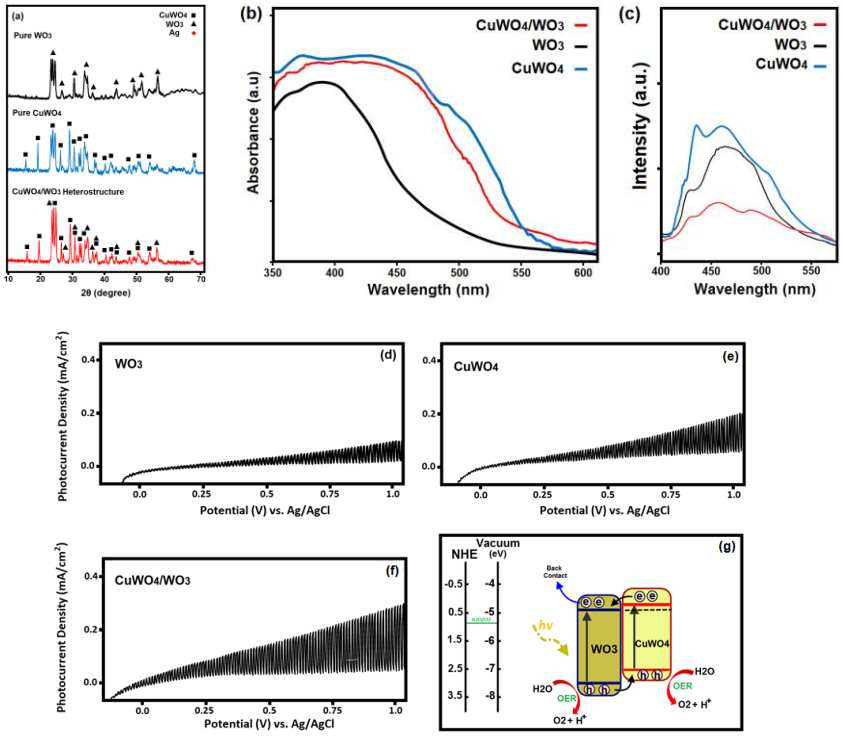


Fig. 3. XRD patterns (a), UV-Vis spectra (b), PL spectra (c) and linear sweep voltammetry (d,e,f) of the obtained products

Thus, compared with other recent reports for similar tungstate-based structures, promising photocurrents were achieved [3-6]. Moreover, based on the obtained data and the calculation of band edges using the method of Ginley and Butler [11], an energy band structure diagram (Fig. 3g) was derived. Clearly an offset between energy levels and the staggered type alignment of the junction reveals that $CuWO_4$ serves as a functional component injecting photo-generated electrons to the CB of $WO_3$ and likewise extracting holes (from the VB of $WO_3$). This alignment and charge transfer allows for a built-in electric field, resulting in an effective charge separation at the interface of the heterojunction, suppressing recombination and consequently enhancing the PEC performance in agreement with the obtained PEC results.

## 4. Conclusions

In summary, $CuWO_4/WO_3$ heterostructured photoanodes were successfully prepared via sol-gel synthesis and electrophoretic deposition. The as-produced composite films exhibited a 2-3-fold higher photocurrent density compared to pristine semiconductors, which was attributed to higher separation efficiency of photo-generated charge carriers, and reduced electron/hole recombination supported by the DFT calculations.

## 5. References


[1] R.V. De Krol, M. Gratzel, "Photoelectrochemical Hydrogen Production" New York; 2012.

[2] H. Sameie, A.A. Sabbagh Alvani, N. Naseri, F. Rosei, G. Mul, B.T. Mei, "Photocatalytic Activity of $ZnV_2O_6$/Reduced Graphene Oxide Nanocomposite: From Theory to Experiment", J. Electrochem. Soc. 165 (2018) H353-H359.

[3] J. Zhu, W. Li, J. Li, Y. Li, H. Hu, Y. Yang, "Photoelectrochemical activity of $NiWO_4/WO_3$ heterojunction photoanode under visible light irradiation" Electrochim. Acta. 112 (2013) 191-198

[4] K.M. Nam, E.A. Cheon, W.J. Shin, A.J. Bard, "Improved Photoelectrochemical Water Oxidation by the $WO_3/CuWO_4$ Composite with a Manganese Phosphate Electrocatalyst", Langmuir. 31 (2015) 10897-10903

[5] D. Bohra, W.A. Smith, "Improved charge separation via Fe-doping of copper tungstate photoanodes, "Phys. Chem. Chem. Phys. 17 (2015) 9857-9866

[6] H. Chen, W. Leng, Y. Xu, "Enhanced Visible-Light Photoactivity of $CuWO_4$ through a Surface Deposited CuO", J. Phys. Chem. C. 118 (2014) 9982-9989.

[7] R. Salimi, A.A. Sabbagh Alvani, B.T. Mei, N. Naseri, S.F. Du," Ag-Functionalized $CuWO_4/WO_3$ nanocomposites for solar water splitting" New J. Chem. 43 (2019) 2196-2203.

[8] R. Salimi, A.A. Sabbagh Alvani, N. Naseri, S.F. Du, D. Poelman,"Visible-enhanced photocatalytic performance of $CuWO_4/WO_3$ hetero-structures: incorporation of plasmonic Ag nanostructures" New J. Chem. 42 (2018) 11109-11116.

[9] M.D Segall, J.D.L. Philip, M.J. Probert, C.J. Pickard, P.J. Hasnip, S.J. Clark, M.C. Payne, "First-principles simulation: ideas, illustrations and the CASTEP code", J. Phys.: Condens. Matter 14 (2002) 2717-2744.

[10] H. Sameie, A.A. Sabbagh Alvani, N. Naseri, S. Du, F. Rosei, "First Principles study on $ZnV_2O_6$ and $Zn_2V2O_7$: Two new photoanode candidate for photoelectronchemical water oxidation", Ceram. Int. 44 (2018) 6607-6613.

[11] M.A. Butler, D.S. Ginley, "Prediction of flatband potentials at semiconductor-electrolyte interface from atomic electronegativitics", J. Electrochem. Soc. 125 (1978) 228-232.